eLIFE
elifesciences.org

Figures and figure supplements

Nup98 FG domains from diverse species spontaneously phase-separate into particles with nuclear pore-like permselectivity

Hermann Broder Schmidt, Dirk Görlich

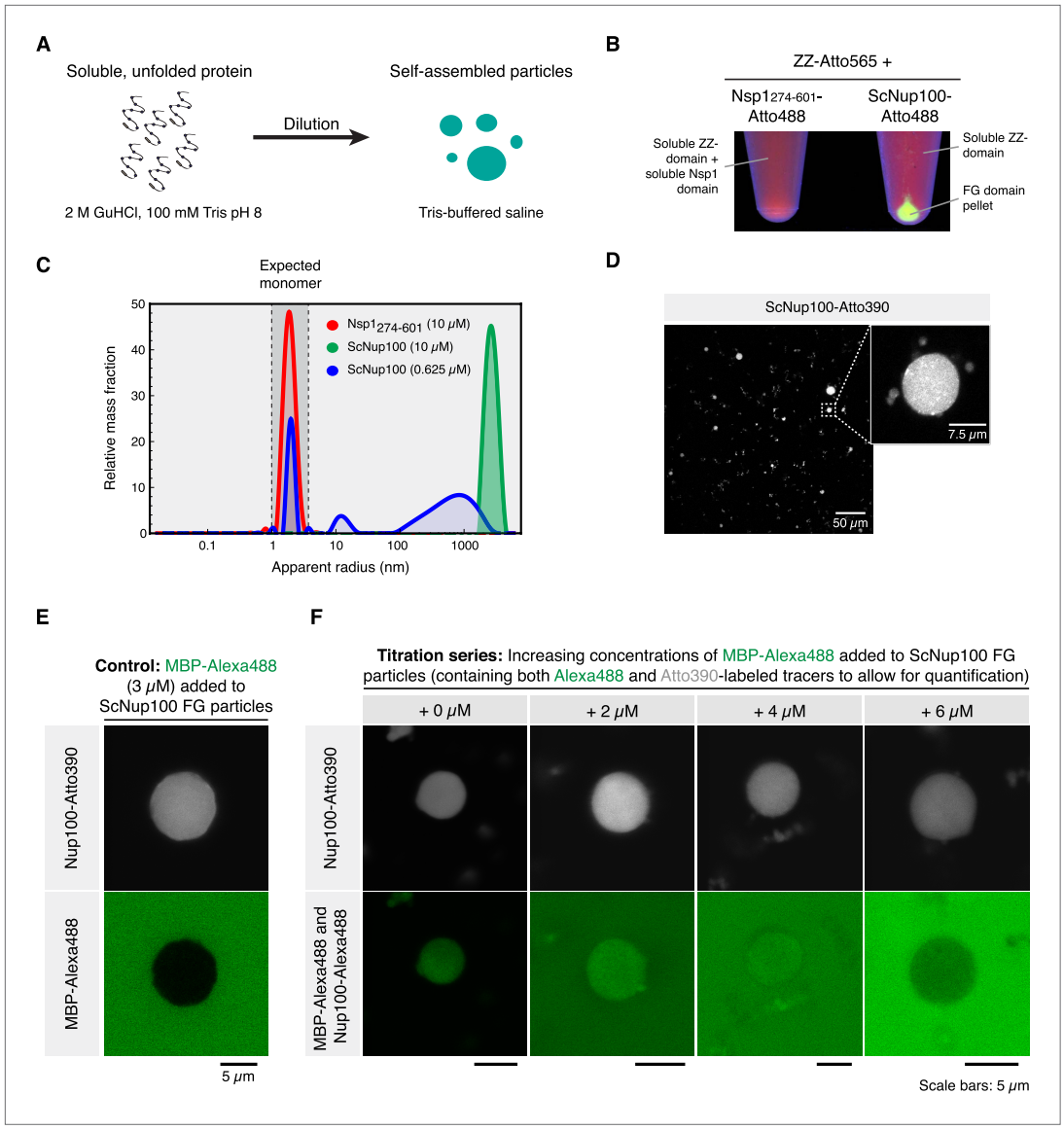

Figure 1. Dilute Nup100 FG domain solutions spontaneously undergo phase-separation. (**A**) Illustration of the experimental design. (**B**) Cohesive FG domains self-assemble into FG phases that can be collected by centrifugation. Two stock protein solutions were prepared in 2 M guanidinium hydrochloride (GuHCl), 100 mM Tris/HCl pH 8.0. They contained 300 μM of a Z-domain tandem fusion (labelled 1:1 with Atto565 maleimide) and 300 μM FG domain from either or Nsp1 (residues 274–601) or Nup100. 5% of the FG domain molecules carried an Atto488 maleimide label. 16.7 μl of each solution was diluted with 500 μl 50 mM Tris/HCl pH 7.5, 150 mM NaCl (TBS). Photographs show test tubes after ultracentrifugation (100,000×*g*, 30 min), illuminated at 366 nm. Note that the Nup100 FG domain pelleted, while the non-cohesive Nsp1 FG repeats and the globular ZZ-domain remained soluble. (**C**) FG particle formation at different concentrations. Label-free $ScNsp1_{276-601}$ and ScNup100 FG domains were diluted from 400 μM stocks (in 2 M GuHCl) to the indicated concentrations with TBS. Formed particles were analysed by Dynamic light scattering (DLS) using a DynaPro NanoStar instrument (Wyatt Technologies). Two data sets, comprising each 100 acquisitions à 5 s, were averaged for each dilution. The Dynamics 7.1.5 software was used for autocorrelation analysis and computation of size distributions. (**D**) Confocal laser-scanning microscopy (CLSM) images showing an overview and zoom-in of ScNup100 FG particles. (**E**) FG particles exclude inert molecules. Particles were formed with 10 μM ScNup100 FG domain and 0.5 μM Atto390-tracer. Particles were mixed with Alexa488-labeled maltose binding protein (MBP), which remained excluded from the particle and thus qualified as an internal standard for Alexa488 fluorescence. (**F**) Estimation of FG domain concentration within FG particles. Particles were formed with 10 μM unlabelled, 0.5 μM Atto390- and 14 nM Alexa488-labelled ScNup100 FG-domain. CLSM images were taken after adding different dilutions of MBP-Alexa488, which served as an internal

Figure 1. Continued on next page

Figure 1. Continued

fluorescence standard. Correlating extra-particle Alexa488 signals (originating from MBP) with the known supplied MBP concentrations and matching them with the intra-particle Alexa488 signals (originating from 1/715th of the FG-domain molecules) suggests that an average particle contains ≈4.5 mM (≈275 mg/ml) FG-domain. This corresponds to ≈200 mM FG motifs.

DOI: 10.7554/eLife.04251.003

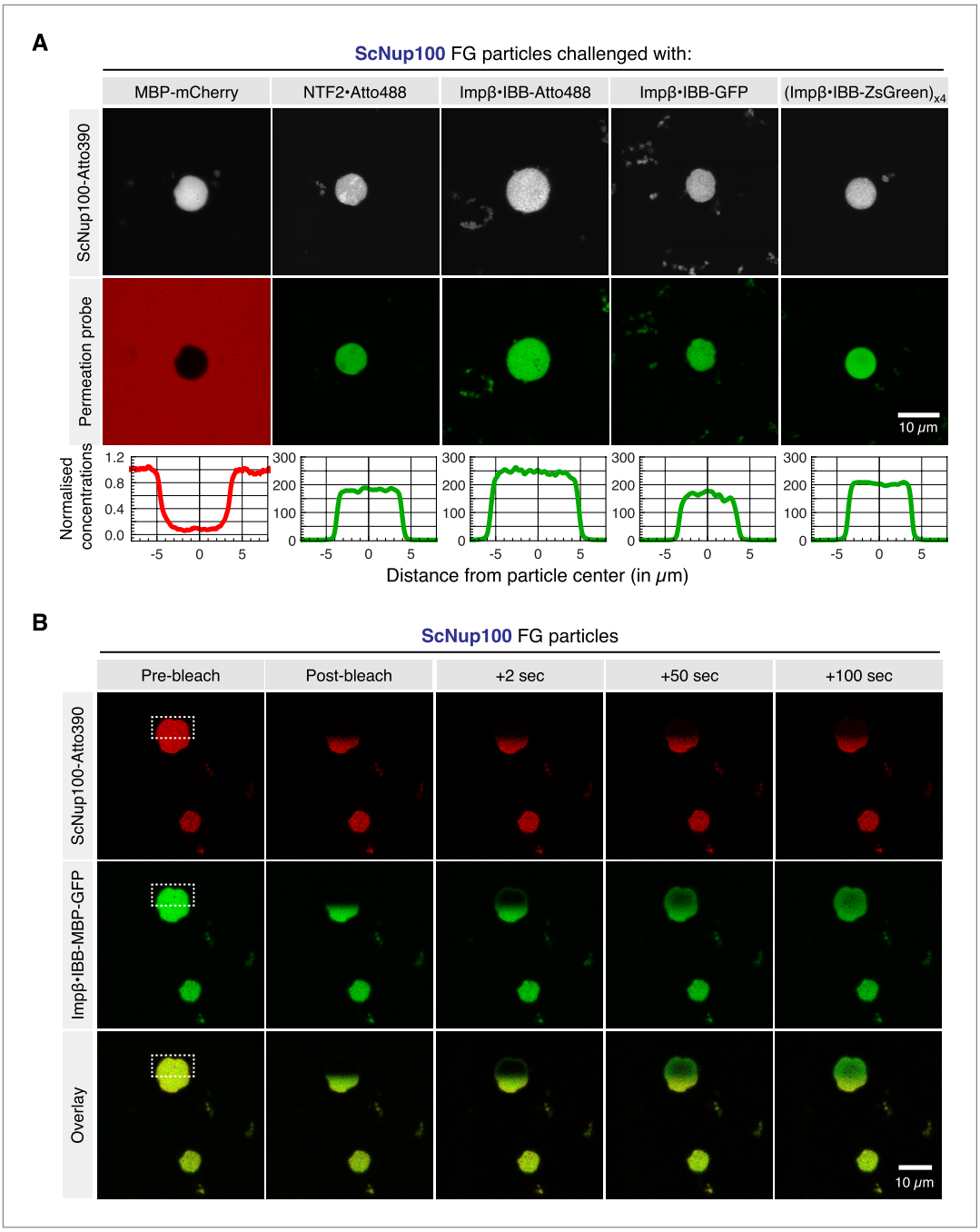

Figure 2. Permeability properties of ScNup100 FG particles. (**A**) FG particles were formed at 10 μM ScNup100 FG domain concentration (including 5% Atto390-tracer), as described above. 3 μM of the passive permeation probe MBP-mCherry or 1 μM of the indicated active permeation species were added (concentration referring to substrate monomers). CLSM images were taken ≈2–3 min later, using the 405 nm, 488 nm, or 561 nm laser lines for exciting the FG tracer, active or passive permeation probes, respectively. (**B**) Intra-FG particle dynamics of FG domains and NTR·cargo complexes. ScNup100 FG particles were formed as in ***Figure 1E*** and challenged with 1 μM of a yeast Impβ•IBB-MBP-GFP complex. CLSM images show two particles. One of them was photobleached at 405 and 488 nm in one hemisphere. Fluorescence recovery of the FG domain tracer as well as of the NTR·cargo complex was detected over time.

DOI: 10.7554/eLife.04251.004

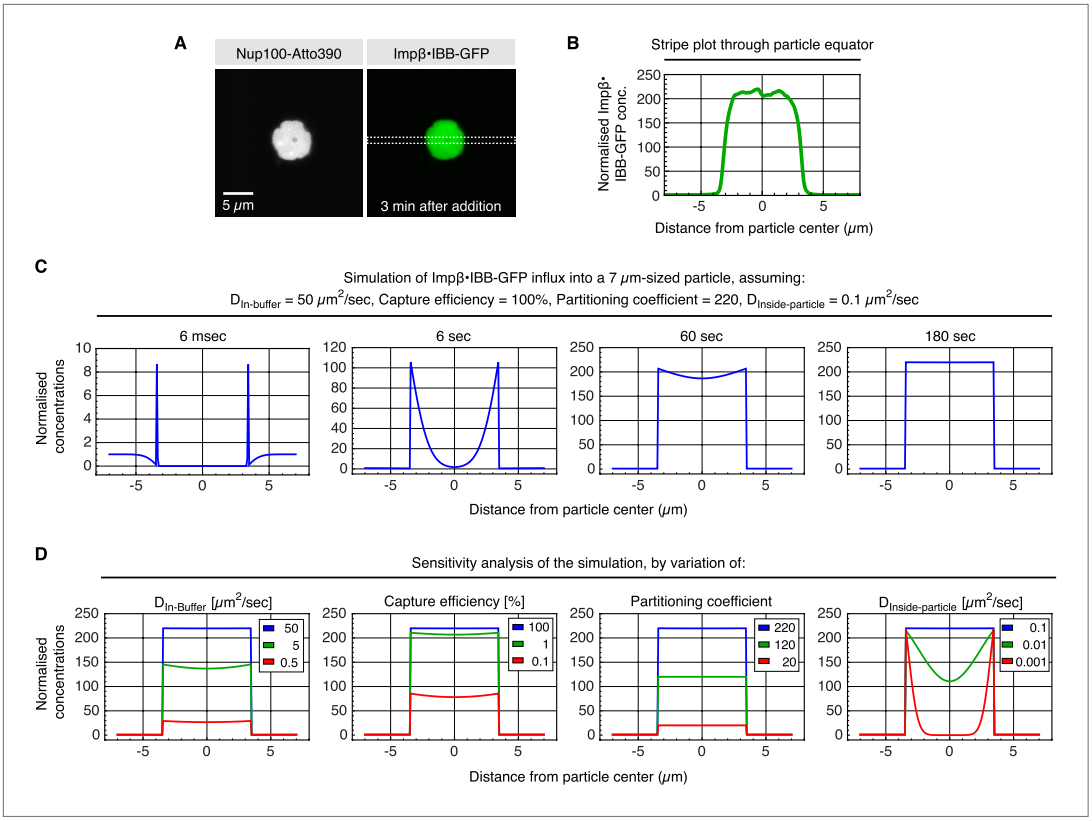

Figure 3. Estimate for kinetic parameters for Importinβ•IBB-GFP influx into ScNup100 FG particles. Influx of the NTR·cargo complex into the FG particles had to be performed in suspension, which implied that we had to wait until particles had settled to the bottom of the slide (≈3 min) before concentration profiles across a particle and surrounding buffer could be recorded. Then, however, the endpoint of accumulation was essentially reached already. In order to nevertheless estimate kinetic parameters for particle-entry, we simulated the process and asked which parameter set would be consistent with the observed cargo distribution at the 3 min time point. These parameters included the partition coefficient (220) and 7 μm particle diameter (both measured directly), the diffusion coefficient in buffer (D_{buffer} = 50 μm²/s, derived by the Stokes–Einstein equation from the radius of the Impβ•IBB-GFP complex and the viscosity of the buffer), as well as the intra-particle diffusion coefficient ($D_{Particle}$ = 0.1 μm²/s), which was the smallest that allowed an even intra-particle distribution of the cargo at the 3 min timepoint. 'Capture efficiency' describes the probability that a colliding NTR·cargo complex gets captured by the particle. Simulations were performed in Mathematica 9.0 and exploited the spherical symmetry of the particle to simplify the system of differential equations (see ***Supplementary file 1*** for the Mathematica code and more detailed explanations). (**A**) ScNup100 FG particles were formed at 10 μM and 30 min later challenged with 1 μM Impβ•IBB-GFP complex. CLSM image was taken after another 3 min. (**B**) Impβ•IBB-GFP concentration profile across the area indicated in panel **A**. Signal was normalized to the concentration in buffer. (**C**) Simulation of influx for indicated parameters and time points. (**D**) Sensitivity analysis, varying the parameters used in **C**. It revealed that diffusion in buffer, the partition coefficient, and diffusion inside the particle, but not the capture efficiency, are limiting for the influx process.

DOI: 10.7554/eLife.04251.005

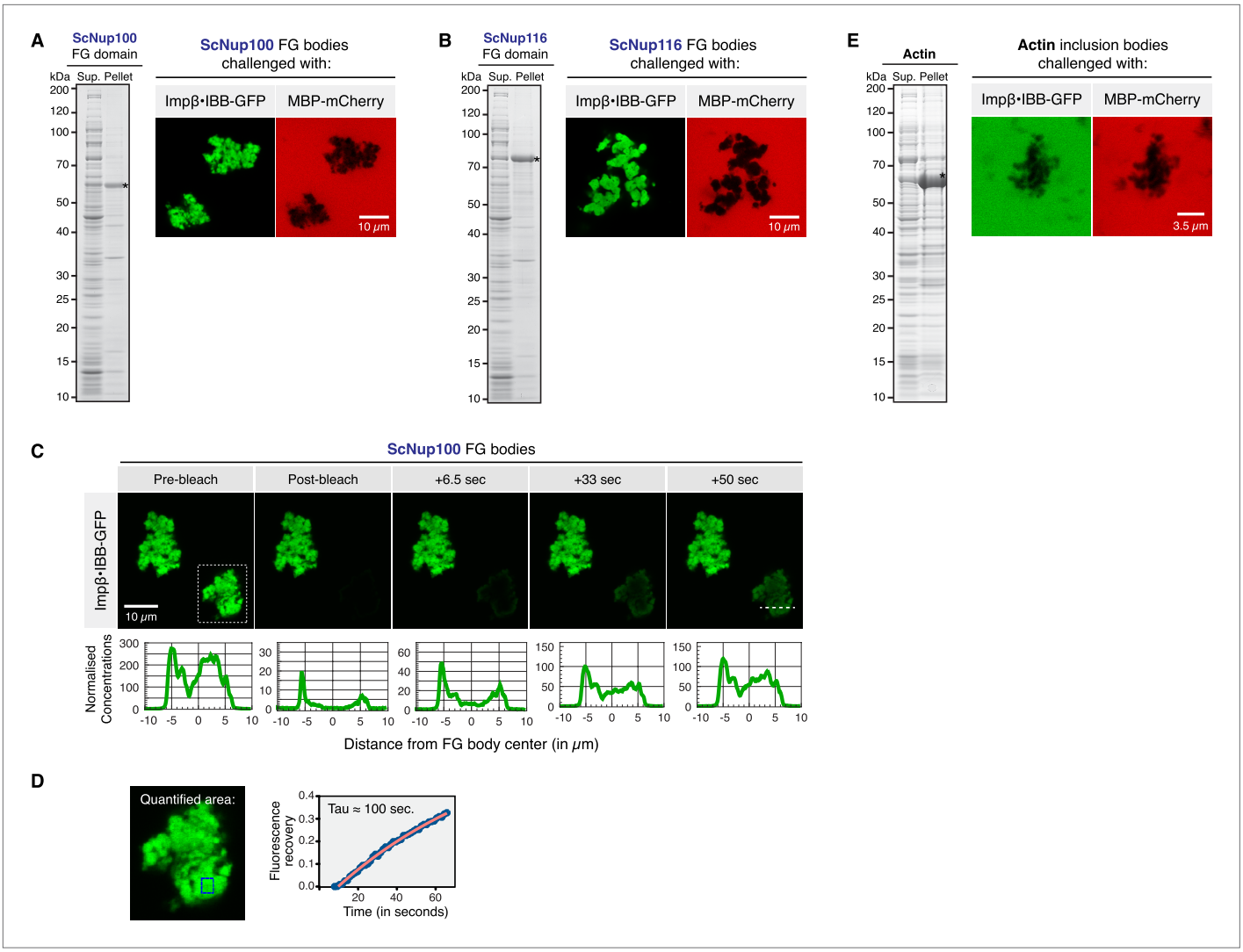

Figure 4. In vivo assembly of selective FG phases. For the undistorted in vivo formation of FG bodies, the ScNup100 and ScNup116 FG domains were expressed in *Escherichia coli* (NEB Express) following induction with 0.5 mM IPTG at 30°C. Cells were pelleted, resuspended in TBS, and lysed with 1 mg/ml lysozyme, 20 μg/ml DNAse I and 0.5% Tween 20. Insoluble 'FG bodies' were recovered by centrifugation at 10,000×*g*. SDS-PAGE analysis of supernatant ('Sup') and pellet fractions and the permeability properties of the recovered ScNup100 (**A**) and ScNup116 (**B**) FG bodies are shown. Crude FG bodies were washed twice in TBS and their permselectivity analysed as described in ***Figure 2***. (**C**) Mobility of NTR•cargo complexes in FG bodies. ScNup100 FG bodies were challenged with 1 μM Impβ•IBB-GFP and photobleached, and fluorescence recovery was detected over time. Note that the NTR•cargo complex was mobile also within the in vivo formed FG bodies. The white dashed line in the 50 s frame indicates the region analysed for the line plots shown below the images. (**D**) Fluorescence recovery over time in the area indicated by the blue box in the zoom-in of the particle outlined by the dashed lines in **C**. The analysed region lies approximately 1 μm inside of the particle. Fluorescence recovery occurred with a time constant of ≈100 s. Note that this involved not only intra-particle diffusion, but also the uptake from the buffer against a ≈200-fold concentration gradient. (**E**) In contrast to the FG bodies, actin inclusion bodies did not enrich the Impβ•IBB-GFP species, but in fact excluded it like MBP-mCherry.

DOI: 10.7554/eLife.04251.008

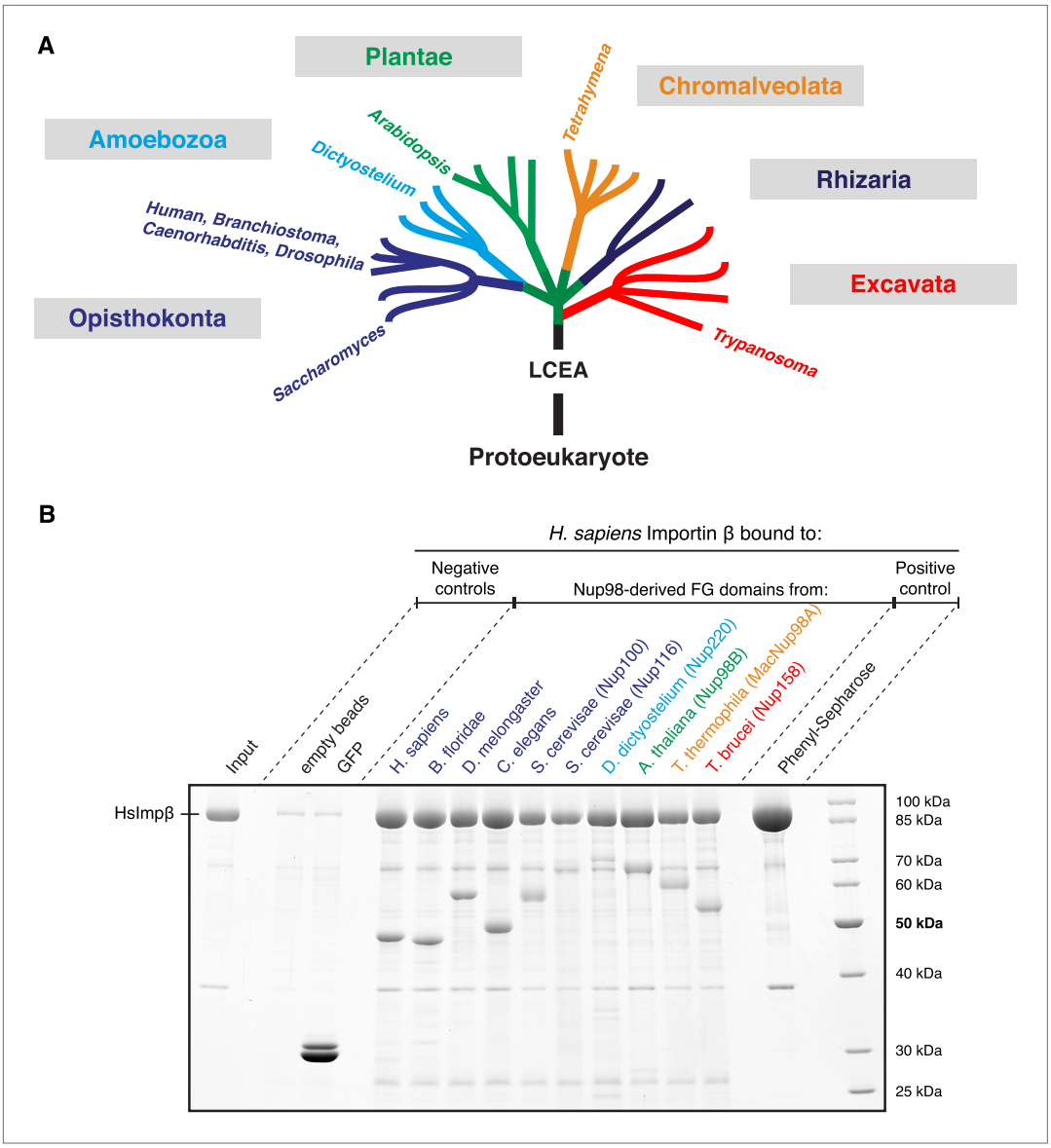

Figure 5. Nup98 FG domains of diverse evolutionary origin bind human Importin β. (**A**) This study analyses ten Nup98 FG domains from nine species. Cartoon illustrates their positions within the eukaryotic tree of life (adapted from ***Keeling et al., 2005***). See ***Supplementary file 2*** for complete sequences. LCEA denotes the position of the last common ancestor to all eukaryotes. (**B**) Indicated His-tagged FG domains (30 µg each) were immobilized on 30 µl PEG-passivated Ni*(ii)* chelate beads and rotated for 2 hr at 4°C with 1 µM untagged human Importin β (400 µl). Bound prey and immobilized baits were co-eluted with SDS/Imidazol and analysed by SDS-PAGE/Coomassie-staining. Note the incomplete elution of the *Saccharomyces* Nup116 and *Dictyostelium* Nup220 FG domains. Phenyl-Sepharose served as a positive control (***Ribbeck and Görlich, 2002***). Binding was in 25 mM Tris/HCl pH 7.5, 100 mM NaCl, 1 mM $MgCl_2$, 0.5% PEG4000, 5 mM DTT.

DOI: 10.7554/eLife.04251.009

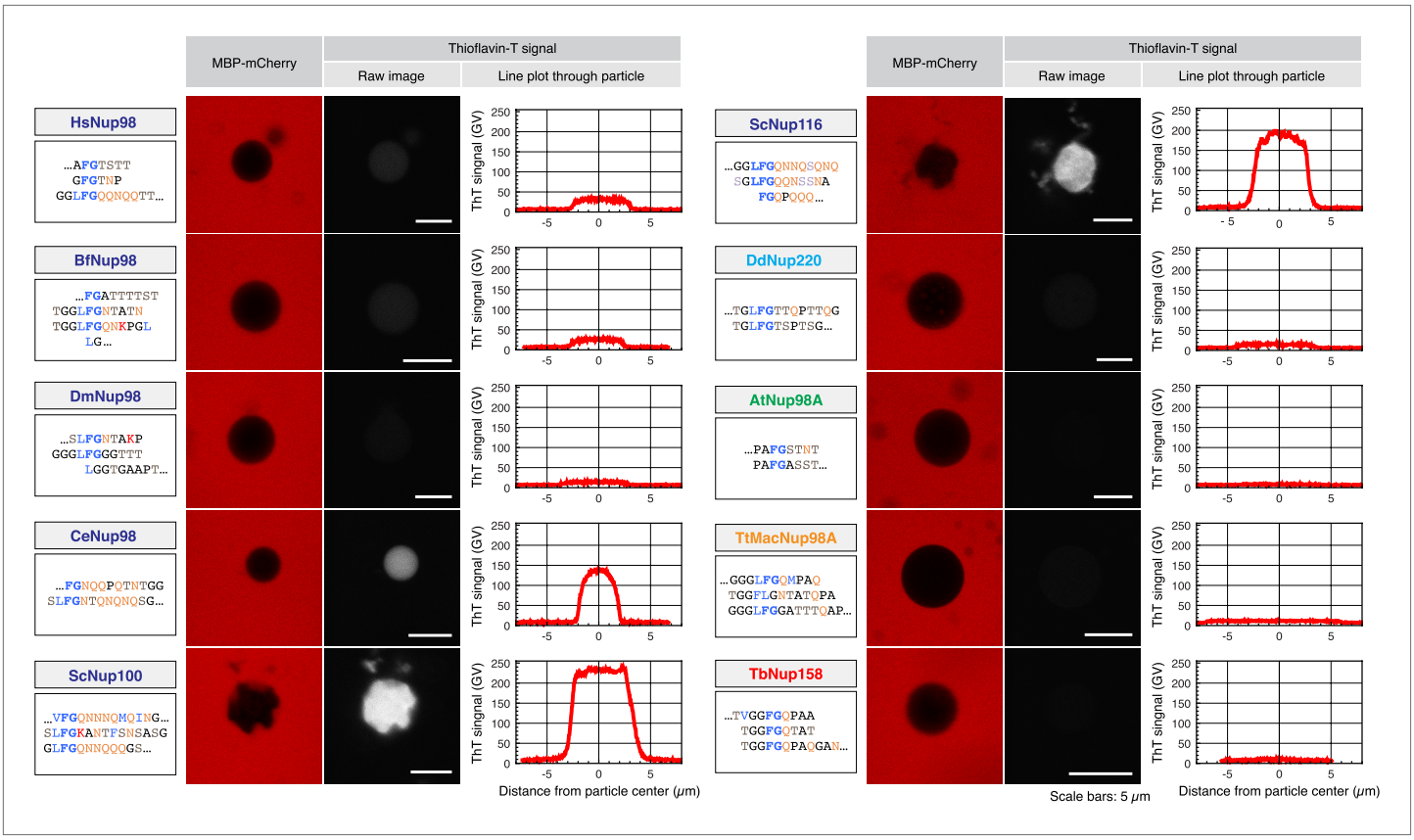

Figure 6. Different modes of inter-FG repeat interactions within FG particles. The indicated Nup98 FG domains were studied. Representative repeat sequences are shown in single letter code (see ***Supplementary file 2*** for complete sequences). Particles were formed at 5 μM (HsNup98, TtMacNup98, TbNup158) or 10 μM FG domain concentration (all other FG domains). The suspensions were afterwards supplemented with 3 μM MBP-mCherry and 1 μM ThioflavinT, a diagnostic dye for the presence of amyloid-like cross-β-structures. Particles were detected based on exclusion of MBP-mCherry. ThioflavinT was excited at 405 nm and detected in a 460–500 nm window. Graphs show quantitations for the measured signals (gray value scales). ScNup100 FG particles gave the strongest signal. For ***Table 1***, all Thioflavin signals were normalized to the Nup100 signal.

DOI: 10.7554/eLife.04251.006

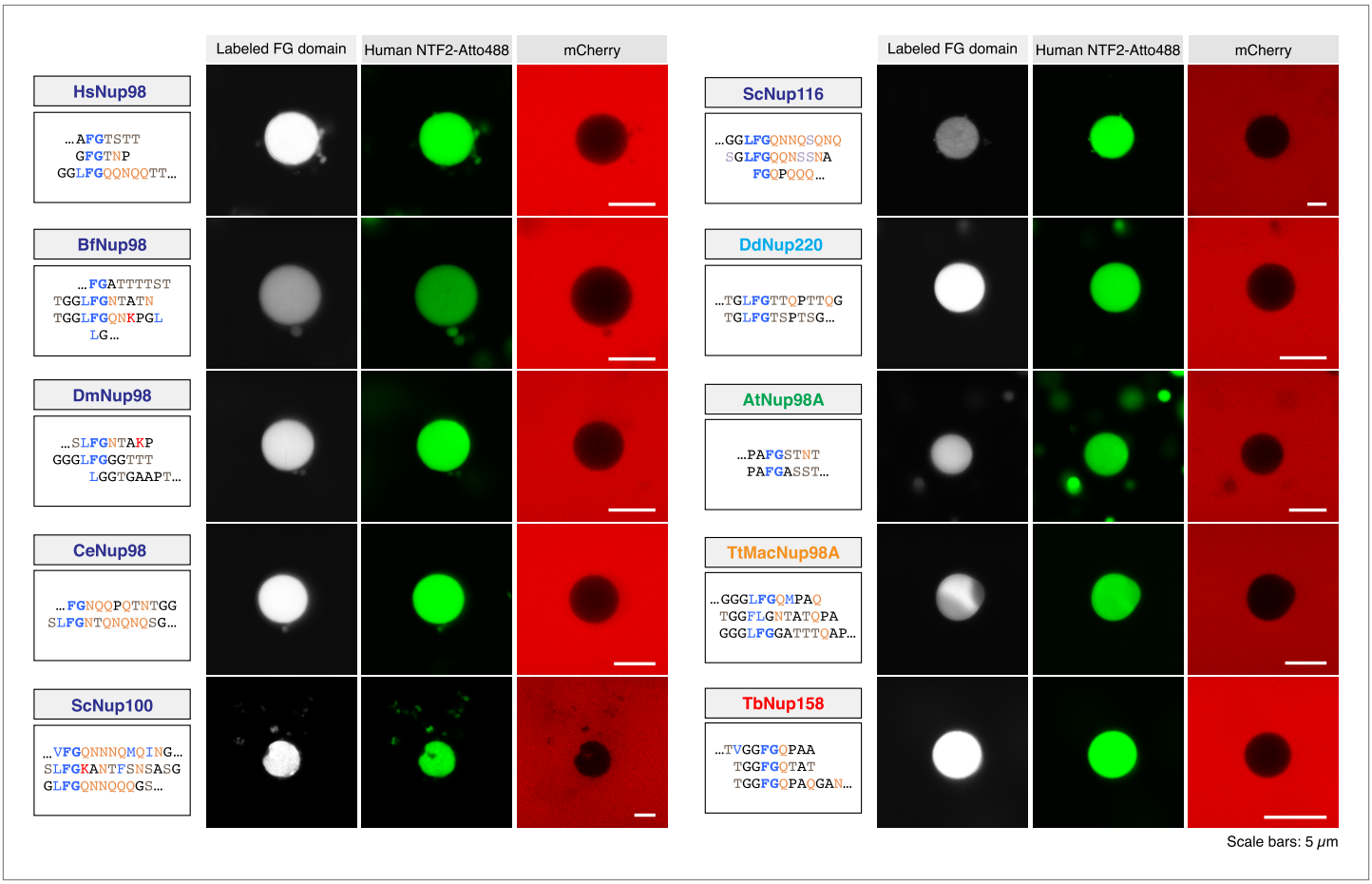

Figure 7. Nup98 FG domains from distant eukaryotic clades self-assemble into highly selective FG particles. Particles were formed as described in ***Figure 6***, followed by the addition of either 1 μM NTF2-Atto488 or Impβ•IBB-GFP and 3 μM mCherry as active and passive permeation probes, respectively. The experimental setup was as in ***Figure 2A***.

DOI: 10.7554/eLife.04251.007

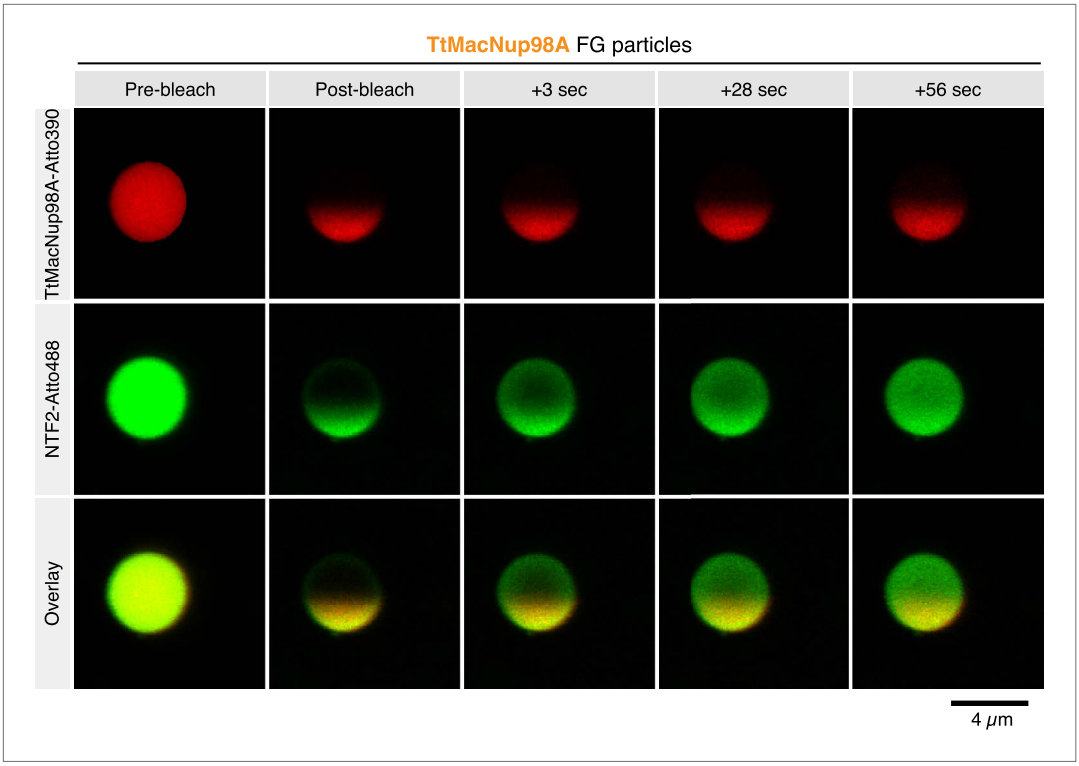

Figure 8. Intra-FG particle dynamics of FG domains and NTRs. TtMacNup98A FG particles were formed with 5 μM unlabeled and 25 nM Atto390-labeled TtMacNup98A FG domain and challenged with 1 μM NTF2-Atto488. 5 min after NTR addition, particles were photobleached at 405 and 488 nm in one hemisphere, and fluorescence recovery of the tracer and NTR followed over time.

DOI: 10.7554/eLife.04251.011

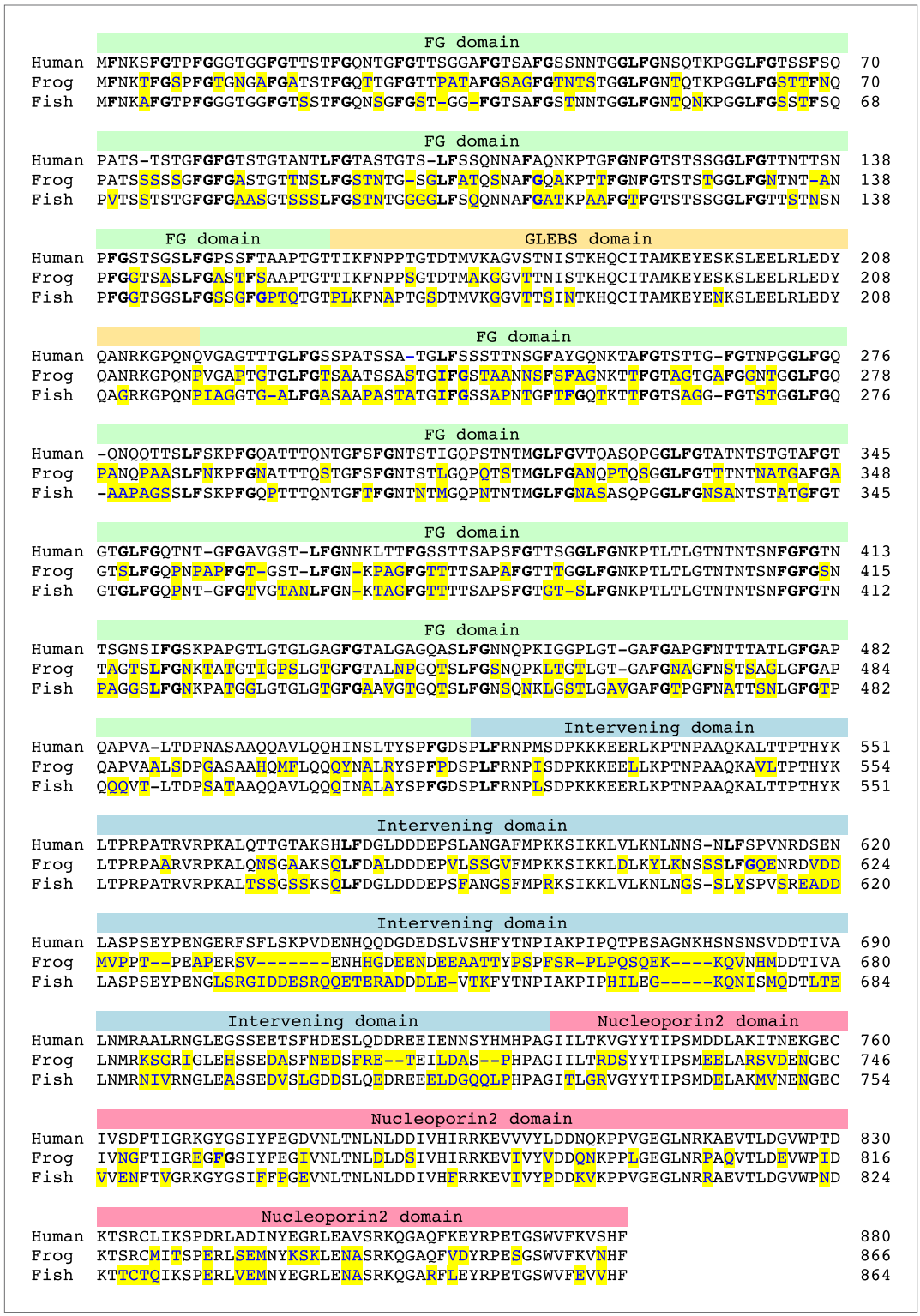

Figure 9. High sequence conservation of the Nup98 FG domain amongst vertebrates. Nup98 from human (GI: 530395413), the frog *Xenopus tropicalis* (GI: 523580018) and the fish *Lepisosteus oculatus* (GI: 573879996) were aligned. FG motifs are in bold; deviations from the human sequence are marked in yellow. The domain structure is annotated. Unlike typical intrinsically disordered domains, the Nup98 FG domain shows a similar conservation (≈70% identity) as the globular, folded nucleoporin2 domain (≈75% identity). The majority of exchanges between the FG domains are very conservative, that is mostly permutations between T, S, N, A, and to a lesser extent, with G. Please also note that many exchanges from the human sequence are identical in frog and fish, further supporting the notion of slow evolution.

DOI: 10.7554/eLife.04251.012

A Initial BLAST searches with three different Nucleoporin2 domain templates

Search template (Species/clade/accession number/Nup98 part)	Identified sequences (with E < 1)
Homo sapiens / Opisthokonta / GI:56549643 / aa:678-863	1024
Arabidopsis thaliana / Plantae / GI:22329468 / aa:887-1027	992
Tetrahymena thermophila / Chromalveolata / GI:289623519 / aa: 786-923	951
Non-redundant sequences:	1037
Putative Nup98 sequences found in all three searches:	913

B Taxonomy report on all identified sequences

Clade	Opisthokonta	Amoebozoa	Plantae	Chromalveolata	Rhizaria	Excavata
Number of sequences	690	12	145	52	2	12

C Domain identification and extraction

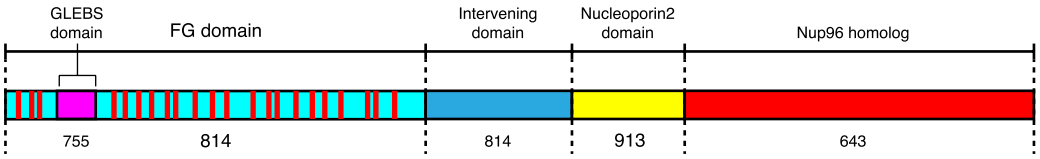

Number of putative Nup98-derived FG domains:	814
FG domains with a length between 400 and 1000 amino acids:	666

D FG dipeptide density

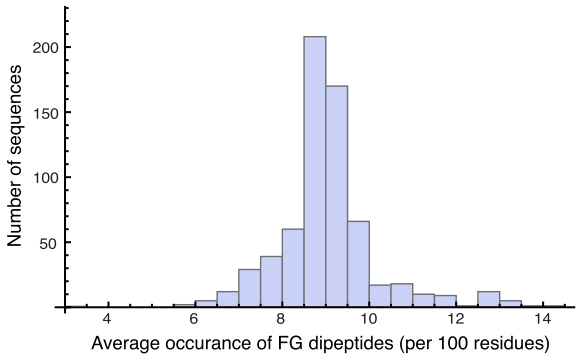

E FG domain composition

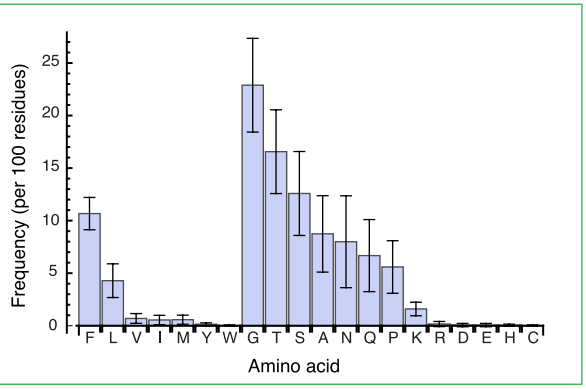

Figure 10. Compilation and analysis of a Nup98 ortholog-derived FG domain database. (**A**) The Nucleoporin2 domains of human Nup98/96 (GI: 56549643), *Arabidopis thaliana* Nup98A (GI: 22329468), and *Tetrahymena thermophila* MicNup98B (GI: 289623519) were used as BLAST templates to identify further Nup98 homologues in the non-redundant NCBI protein database. The 913 sequences identified in all three searches were then analysed further as subsequently described. (**B**) Taxonomic classification of identified full-length Nup98 candidates. (**C**) Cartoon illustrates domain structure of a canonical Nup98-Nup96 fusion protein that includes an FG repeat domain, an embedded Gle2p-binding site (GLEBS domain), an intervening domain, the Nucleoporin2 domain, as well as the Nup96 part. The number of Nup98 candidates that comprise a given module is written underneath. (**D**) FG domains included residues from translation start till the last FG dipeptide but excluded the GLEBS domain (as defined by alignment with the ScNup116 GLEBS domain). For subsequent analyses, only the 666 FG domains with 400–1000 residues were considered. The histogram illustrates the FG dipeptide density distribution with a median of 9 FG dipeptides per 100 residues (or one FG dipeptide per 11 residues). Outliers to higher densities (>10 FG/100 residues) mainly represent domains dominated by less hydrophobic FG motifs (e.g. GFGQ motifs) than the often dominating LFG motifs. (**E**) Average amino acid composition of Nup98 FG domains and corresponding standard deviations. Note that the inter FG spacers are dominated by G, T, S, A, N, Q, and P, while F and L dominate the hydrophobic residues. F shows the smallest coefficient of variation.

DOI: 10.7554/eLife.04251.014

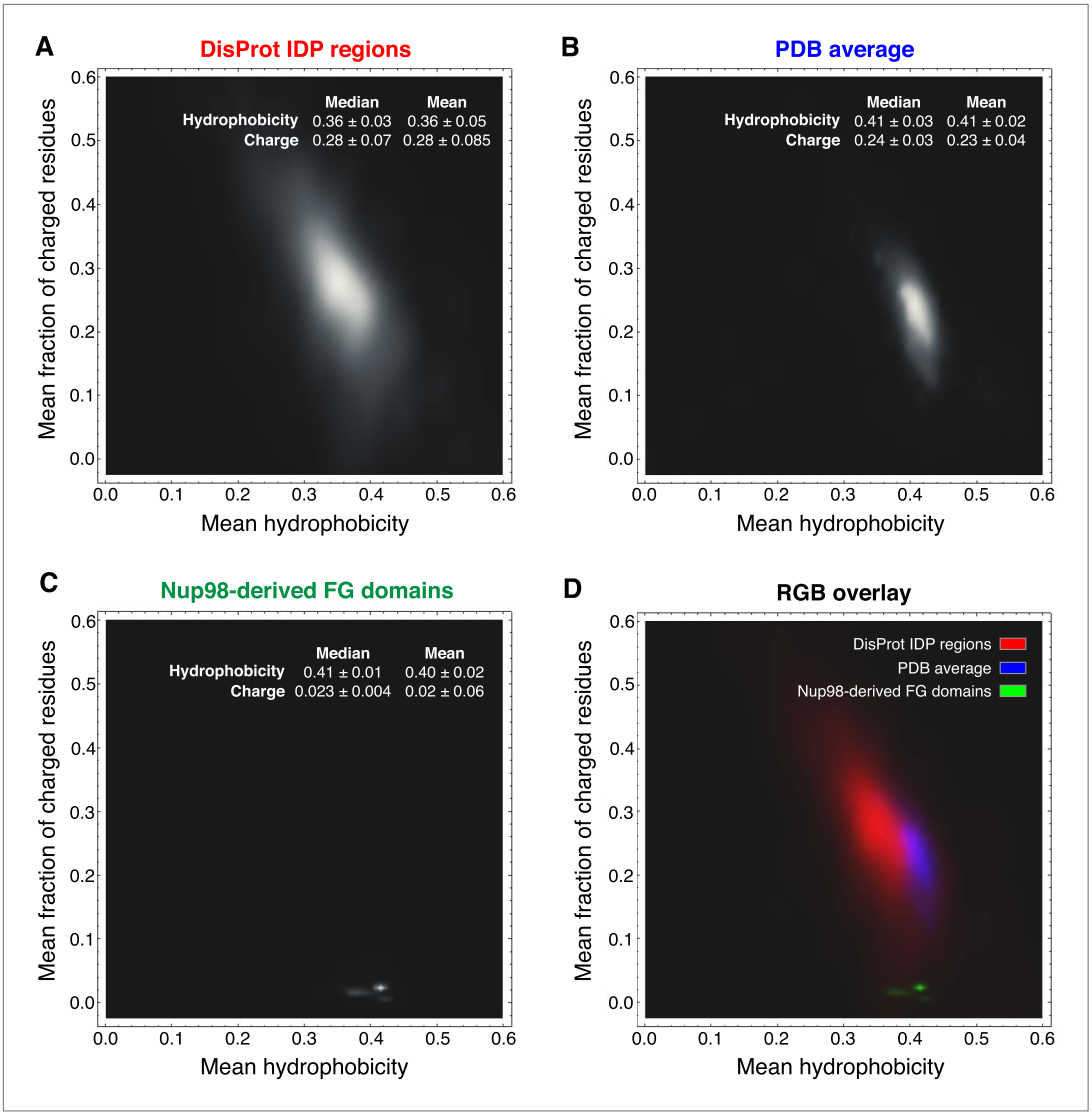

Figure 11. Comparison of Nup98 FG domains to intrinsically disordered and globular proteins in terms of charged residue contents and hydrophobicity. Analysis was similar to ***Uversky et al. (2000)***, the differences being (i) that we considered not the net charge, but the total fraction of charged residues and (ii) we used a more strictly defined hydrophobicity scale that is not biased by globular protein structures. For each protein sequence, the mean fraction of charged residues was determined by counting D, E, K, and R and dividing this sum by the sequence length. Mean hydrophobicity was calculated according to a scale based on partitioning of Nα-acetyl-amino acid amides between 1-octanol and water at neutral pH (given in ***Table 2*** in ***Fauchere and Pliska, 1983***). For clarity, we re-scaled their numbers linearly to range between 0 and 1, and thus used the following parameters: (R, 0); (K, 0.006); (D, 0.012); (E, 0.113); (N, 0.132); (Q, 0.242); (S, 0.298); (G, 0.31); (H, 0.35); (T, 0.39); (A, 0.405); (P, 0.46); (Y, 0.604); (V, 0.684); (M, 0.687); (C, 0.782); (L, 0.831); (F, 0.859); (I, 0.862); (W, 1). The brightness in the heat maps reflects the number of proteins in a given regime of the plot. (**A**) 667 intrinsically disordered protein (IDP) regions were extracted from the DisProt database (***Sickmeier et al., 2007***) and analysed as described above. Note their wide distribution in the plot, their high content of charges residues and low hydrophobicity. (**B**) Analysis of 34,551 non-redundant protein sequence entries from the PDB (***Bernstein et al., 1978***), representing mostly globular, folded proteins. Note that these sequences are on average less charged and considerably more hydrophobic than the bulk of IDPs. (**C**) Analysis of the 666 identified Nup98 FG domains (excluding the GLEBS domain). Despite also being intrinsically disordered, they strongly cluster in a very narrow region with extremely very low charge density and a hydrophobicity very close to globular proteins. The few outliers with slightly less hydrophobicity represent NQ-rich sequences and reflect the facts (i) that N and Q are more hydrophilic than other typical inter-FG spacer residues (A, T, S, G, P) and (ii) probably that NQ-rich stretches contribute to cohesiveness by conferring very

Figure 11. Continued on next page

Figure 11. Continued

hydrophilic (cross-β) contacts (***Ader et al., 2010***). (**D**) For direct comparison, plots A (in red), B (in blue), and C (in green) were overlaid in a single plot.

DOI: 10.7554/eLife.04251.015

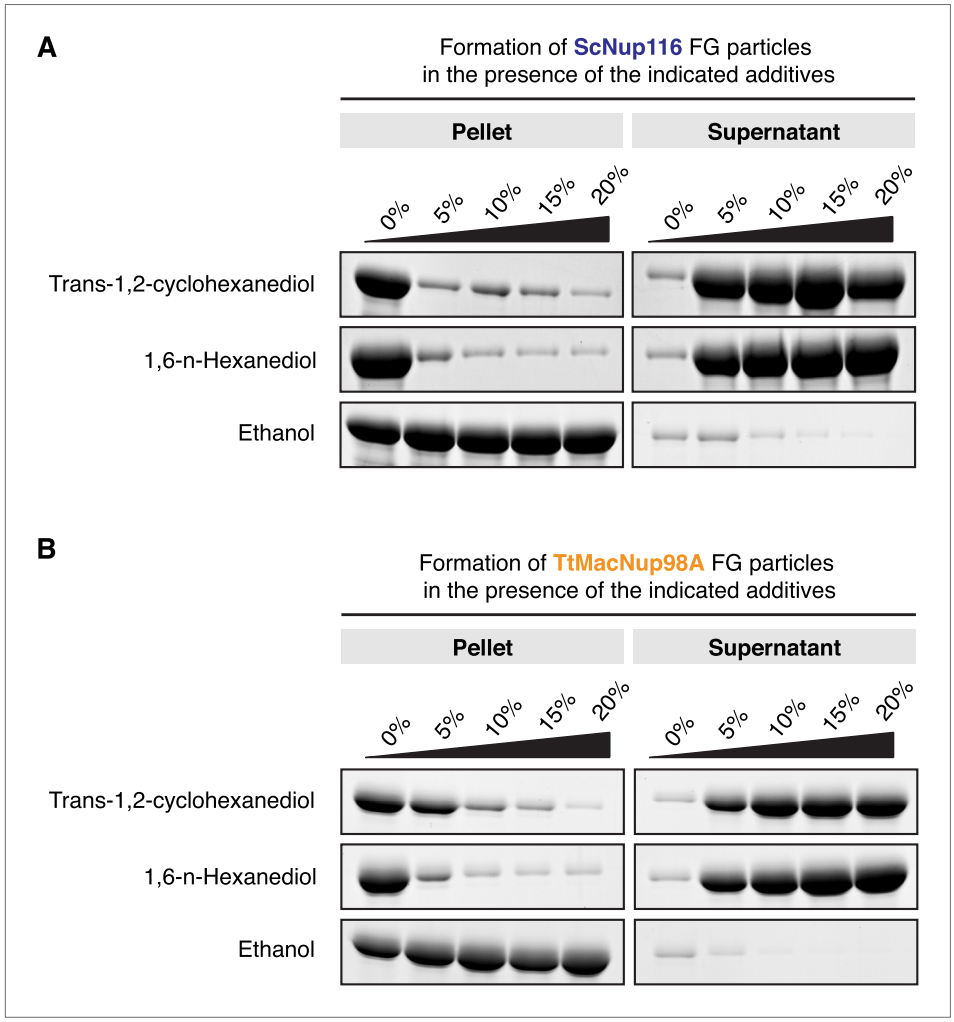

Figure 12. Influence of hexanediols on FG particle formation. FG particles were assembled in a volume of 200 µl with 10 µM ScNup116 (**A**) or TtMacNup98A (**B**) FG domain in the presence of increasing amounts of *trans*-1,2-cyclohexanediol, 1,6-hexanediol or ethanol. After 60 min of incubation, formed particles were collected as pellets in a 10-min 20,000×*g* centrifugation step. They were analysed together with the soluble supernatants by SDS-PAGE. Both hexanediols clearly disrupted the FG particles, though TtMacNup98A FG particles appear slightly more resistant than ScNup116 FG particles (consistent with the lower saturation concentration of the Mac98A FG domain). In contrast, ethanol had no disruptive effect, but rather precipitated the FG domains.

DOI: 10.7554/eLife.04251.016

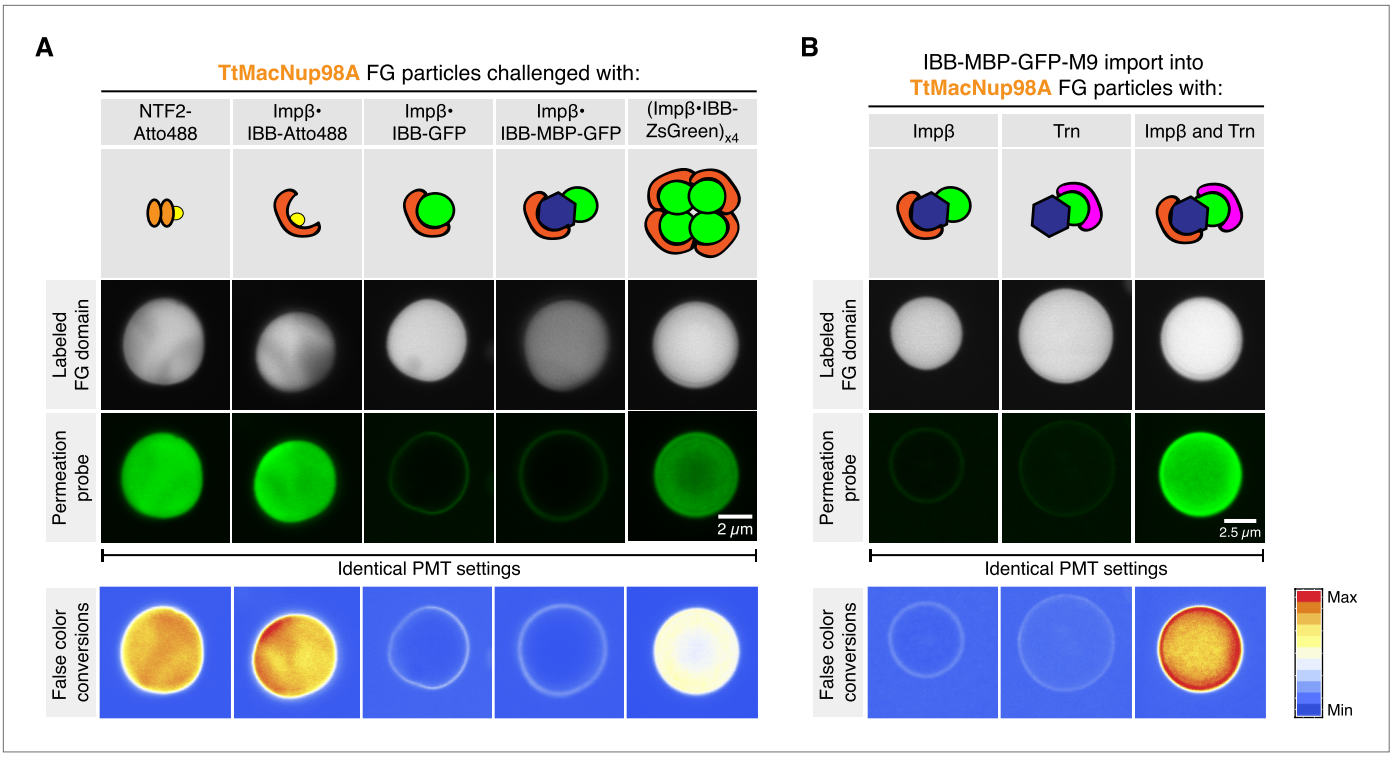

Figure 13. Effect of cargo domains and NTR stoichiometry on entry into TtMacNup98A FG particles. FG particles (with 5% Atto390-labeled tracer) were formed with 5 μM TtMacNup98A FG domain. CLSM images show how NTR·cargo complexes of different sizes and NTR-to-cargo ratios partition between FG phase and bulk solvent. IBB (recognized by Importin β) and M9 (recognized by Transportin, Trn) represent two orthogonal nuclear import signals. See ***Figure 13—figure supplement 1*** and main text for additional information.

DOI: 10.7554/eLife.04251.017

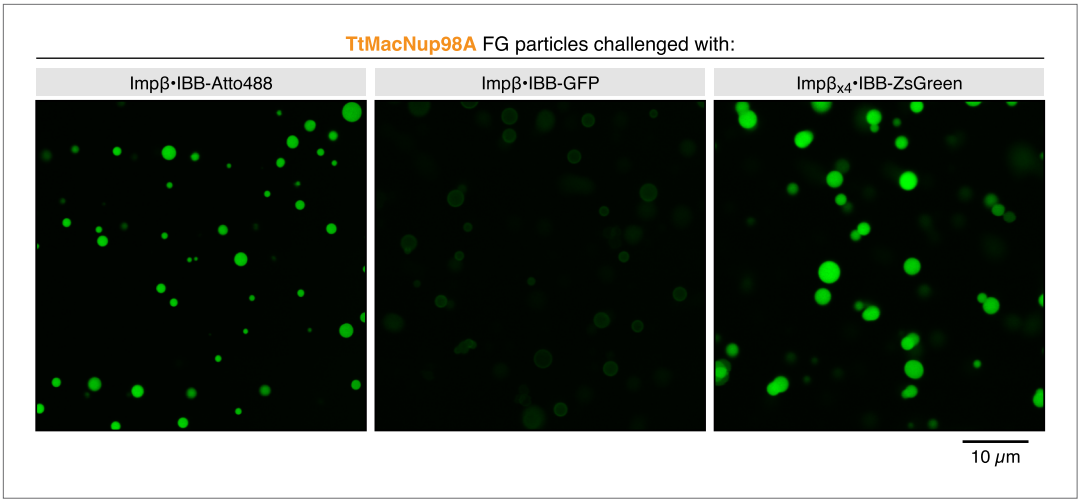

Figure 13—figure supplement 1. Partitioning of various NTR cargo complexes into TtMacNup98 FG particles. The experiment is identical to the corresponding panels of ***Figure 13***, the only difference being that a larger field and more particles were imaged at a lower resolution. This was done in order to document that the described differences apply to entire particle populations.

DOI: 10.7554/eLife.04251.018

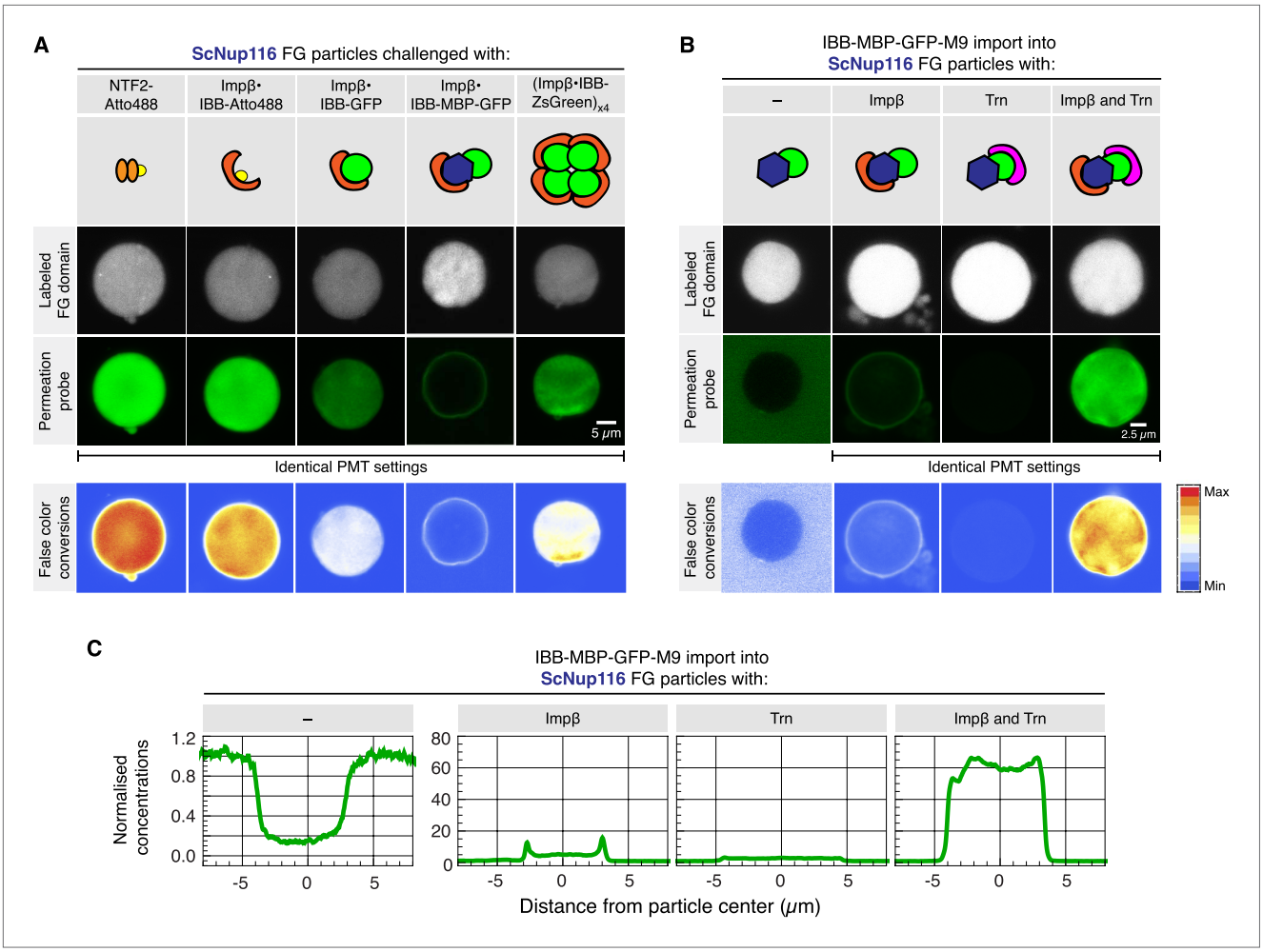

Figure 14. Effect of cargo domains and NTR stoichiometry on entry into ScNup116 FG particles. FG particles (with 5% Atto390-labeled tracer) were formed with 10 μM *S. cerevisiae* Nup116 FG domain. See ***Figure 13*** and main text for additional information.

DOI: 10.7554/eLife.04251.019

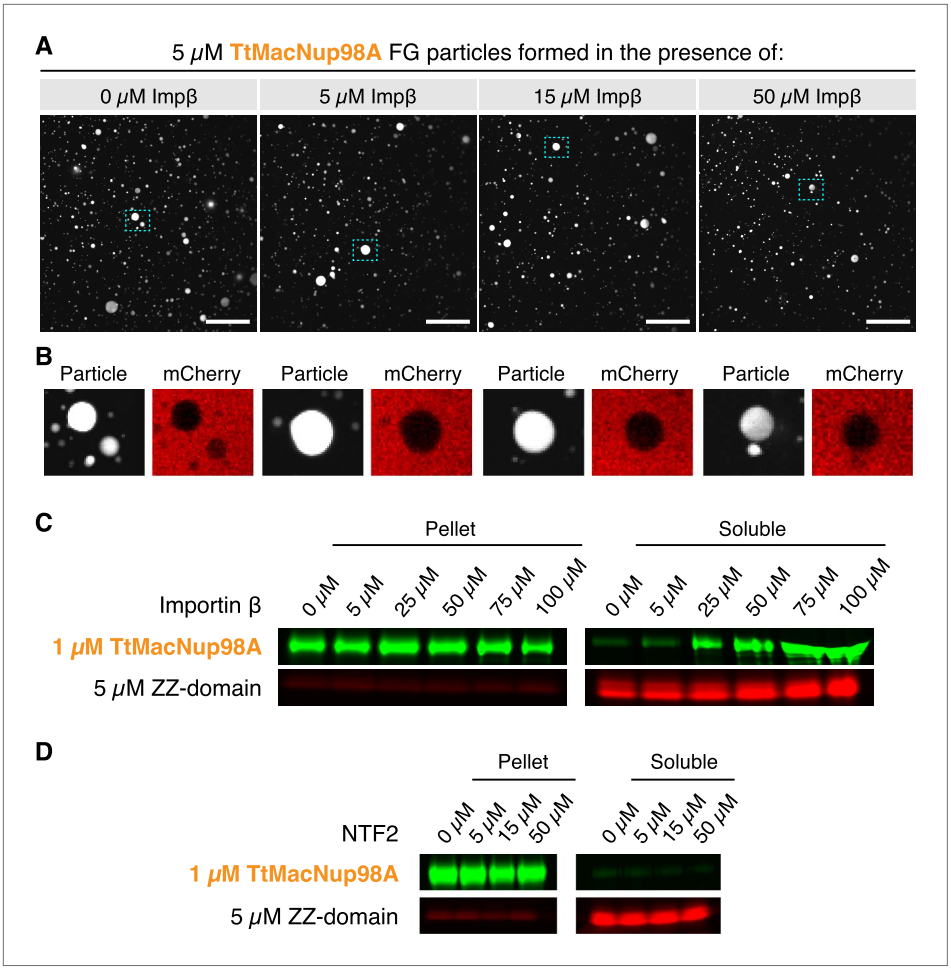

Figure 15. Formation of FG particles in the presence of NTRs. (**A**) NTRs do not suppress FG particle formation at molar ratios expected within NPCs. FG particles were formed by dilution of TtMacNup98A to 5 μM (including 5% Atto390-labeled tracer) with Tris-buffered saline containing the indicated concentrations of Importin β. Approximately, 60 s after particle formation, 3 μM mCherry was added. The CLSM images show that FG particles can still form in the presence of a 10-fold molar excess of NTRs. (**B**) An excess of NTRs does not compromise barrier function. Zoom-ins on the particles indicated in **A** show that mCherry is excluded in all cases. (**C**) Importin β increases the critical concentration for FG particle formation only when added in very high excess. FG particles were formed by dilution of TtMacNup98A to 1 μM (including 5% Atto488-labeled tracer) with Tris-buffered saline containing 5 μM Atto565-labeled ZZ-domain and the indicated concentrations of Importin β. After 10 min of incubation, particles were collected by ultra-centrifugation at ≈125,000×*g* for 1 hr, and the amount of FG domains in the pellet and supernatant analysed by SDS-PAGE. For detection of the labelled FG domains, a Fujifilm FLA-9000 fluorescence imager was used. (**D**) Unlike Importin β, NTF2 does not influence the critical concentration of FG particle formation. Experimental setup as in (**C**), with the exception that TtMacNup98A FG particles were formed by dilution with buffer containing the indicated concentrations of NTF2.

DOI: 10.7554/eLife.04251.020